Applied Catalysis B: Environment and Energy 356 (2024) 124219

Contents lists available at ScienceDirect

Applied Catalysis B: Environment and Energy

journal homepage: www.elsevier.com/locate/apcatb

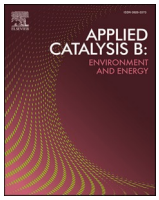

Complete removal of *N*-nitrosamines using in-situ constructed sequential microreactors: Synergies of catalysis-adsorption between *N*-nitrosamines and their degradation products

Zifan Liu [b], Yu Meng [a], Yue Wang [a], Zepeng Zhang [b], Zhonglong Yin [a], Yong Dai [c], Fuqiang Liu [b], Weiben Yang [a,*]

[a] School of Chemistry and Materials Science, Jiangsu Collaborative Innovation Center of Biomedical Functional Materials, Nanjing Normal University, Nanjing 210046, China
[b] State Key Laboratory of Pollution Control and Resource Reuse, School of the Environment, Nanjing University, Nanjing 210023, China
[c] School of Chemistry and Chemical Engineering, Yancheng Institute of Technology, Yancheng, China

ARTICLE INFO

Keywords:
N-nitrosamine
Peroxonosulfate activation
Adsorption
$NiCo_2O_4$-nanoarray
Sequential microreactor

ABSTRACT

The removal of *N*-nitrosamines from water faces the challenges of their difficult adsorption, and incomplete mineralization of degradation products. Herein, we report a new strategy by in-situ constructing microreactor on carbon cloth arrayed CoNi spinel oxide through membrane encapsulation. The $NiCo_2O_4$-nanoarrays activate peroxonosulfate, generating reactive oxygen species that rapidly degrade *N*-nitrosamines. The breaking N-N bond of *N*-nitrosamines provides an effective binding site for adsorbing degradation products (secondary amines). Meanwhile, electrons conducted from secondary amines adsorbed on Ni sites reconstruct the charge of CoNi sites, bolstering the peroxonosulfate activation to further remove *N*-nitrosamines and secondary amines. Moreover, the microreactive interface formed between membrane substrate and $NiCo_2O_4$-nanoarrays improved the reaction efficiency. It maintains efficient *N*-nitrosamines removal (96–99%) even in the presence of humic acid. Actual wastewater experiments confirmed its effective control of both *N*-nitrosamines and *N*-nitrosodimethylamine formation potential. This study provides a novel approach for eliminating the risk of N-nitrosamines in water.

1. Introduction

The increase in industrial production and human activities has put pressure on the current water treatment system. Furthermore, this issue has become more severe due to the continuous emergence and increasing severity of emerging pollutants. *N*-nitrosodimethylamine (NDMA) and other *N*-nitrosamines, nitrogen-containing micropollutants, are mainly derived from industrial production and the conversion of precursors in chloramine disinfection processes [1,2]. Their carcinogenicity and mutagenicity have attracted strong public attention.

Adsorption, a common treatment technology, works on the removal of many micropollutants. However, it is difficult to effectively adsorb *N*-nitrosamines due to their low molecular weight and uncharged feature [3–5]. Advanced oxidation processes (AOPs), such as ozonation, UV/hydrogen peroxide, and photocatalysis, are considered promising treatment methods for wastewater and can indeed effectively degrade *N*-nitrosamines by generating strong reactive oxygen species [4,6–9]. Although no studies have been reported, AOPs based on peroxonosulfate (PMS) might show excellent removal effect on *N*-nitrosamines due to their easy activation and higher oxidation potential of sulfate radicals [10,11]. On the other hand, byproducts like dimethylamine (DMA) generated from the oxidation of *N*-nitrosamines or nitrogen-containing pollutants, as precursors, still pose a risk of conversion to *N*-nitrosamines [1,7]. Therefore, the treatment of byproducts needs careful consideration to prevent the rebirth of *N*-nitrosamines. Fortunately, some adsorbents can efficiently remove *N*-nitrosamine precursors [7,12,13]. Related research has also achieved effective removal of NDMA and DMA through cyclic coupling of photocatalysis and adsorption processes [6]. However, the long reaction time and many interfering factors greatly restrict the control of *N*-nitrosamines during segmented treatment and inevitably lead to increased costs. Rapidly, efficiently, and completely removing *N*-nitrosamines through integrated technology

* Corresponding author.
E-mail address: yangwb007@njnu.edu.cn (W. Yang).

https://doi.org/10.1016/j.apcatb.2024.124219
Received 29 February 2024; Received in revised form 28 April 2024; Accepted 19 May 2024
Available online 21 May 2024

remains a challenge.

Transition metals and their oxide materials, as common types of catalytic materials, can easily activate PMS [14,15]. Moreover, previous studies have shown that metal oxides and hydroxides such as Cu and Ni have good adsorption performance for nitrogen-containing pollutants such as DMA and ammonia nitrogen [12,16]. Therefore, materials designed with combinations of different metals that balance their catalytic and adsorption properties can enable them to synergistically promote the simultaneous removal of *N*-nitrosamines and their precursors. However, functional nanomaterials themselves have barriers in water treatment due to their ultrafine powder characteristics [17]. Moreover, uncontrollable mass transfer in packed bed reactors and the interference of macromolecular pollutants in water both significantly affect inherent catalytic and adsorption performance [18,19].

Recently, membrane-based reactors have attracted widespread attention [20,21]. First, the membrane layer can block the interference of macromolecular pollutants such as natural organic matter (NOM) [22]. Second, the microreactive interface between membrane substances and nanomaterials can also improve mass transfer for the rapid removal of pollutants [20,22,23]. According to previous reports, nanomaterials are mainly fixed on membranes through blending and surface coating. However, these methods either only integrate the material onto the membrane surface or fail to control the position of the materials on the membrane [20,22,24]. Surface materials cannot avoid interference from large molecules, potentially leading to harmful disinfection byproducts from NOM in AOPs [25,26]. The uncontrollable distribution of materials in membrane reactors leads to unstable performance. Considering this, some studies have proposed a strategy of sequential membrane construction, which effectively solves the problem of multiple pollutants in water [27]. Although most of the reported membranes have little effect on NDMA removal [5,7], materials designed based on the above concept may have the potential to effectively control *N*-nitrosamines in wastewater.

To solve the problems mentioned above, we invented a microreactor named UCAM (ultrafiltration-catalysis/adsorption microreactor), a reasonable and regulable design with an ultrafiltration-catalysis/adsorption structure, relying on CoNi spinel nanoarrays scattered on carbon fiber cloth, for catalysis-adsorption synergistic removal and control of *N*-nitrosamines. Carbon cloth (CC) has a relatively regular structure, which results in in situ-loaded nanomaterials having an ordered distribution. Its three-dimensional network structure allows the dispersed material to have good mass transfer effects in flow mode. Meanwhile, carbon fiber cloth as a support layer is also a good carrier for membrane encapsulation. The separation layer, formed by membrane encapsulation at the top of the microreactor, can suppress NOM in advance, ensuring efficient AOPs and adsorption processes. Moreover, with the microscale channel of the membrane matrix, the microreactor constructed on the $NiCo_2O_4$-nanoarrays greatly improved the synergistic catalysis-adsorption performance. The efficiency and practical ability of UCAM for PMS activation to degrade *N*-nitrosamines and adsorb precursors in their degradation products were evaluated through the treatment of simulated water and real wastewater. Experiments, characterization and theoretical calculation were carried out to reveal the degradation and adsorption mechanisms of *N*-nitrosamines and their products in PMS activation system, and the synergistic mechanism between catalysis and adsorption was explored in detail. This work provides a catalytic-adsorption integrated strategy for the complete control of *N*-nitrosamines, while utilizing a new membrane based microreactor to achieve more rapid and efficient removal of micropollutants in complex water environment.

2. Materials and methods

2.1. Materials

All reagents used in this work were of analytical grade without further purification and the details are described in the supporting information (SI) in Text S1. Carbon fiber cloth (CC) and cotton cloth (CTC) were purchased from Taiwan Carbon Energy Technology Co., Ltd, China, and Nanjing Clothing Factory, China, respectively. The cotton cloth was calcined at 400℃ in a nitrogen atmosphere for 2 hours. Wastewater samples were collected in June 2023 from an industrial wastewater treatment plant and an urban domestic wastewater treatment plant in Nanjing, China. The selected urban domestic wastewater treatment plant treatment processes included coagulation, oxic processes, ultrafiltration membrane filtration and industrial wastewater treatment plant included coagulation, anoxic/oxic processes, membrane bioreactors. In the real water experiment, samples were collected from the secondary effluent after activated sludge processes. The samples were kept in 10 L mild cleaned plastic bottles, and stored in the refrigerator at 4℃ before use. The pretreatment included filtration through a 0.45 μm cellulose triacetate membrane filter. The characteristics of the raw surface water are provided in Table S1.

2.2. Synthesis of CC/CTC with $NiCo_2O_4$ nanoarrays

Briefly, 1 g of $Ni(NO_3)_2{\cdot}6\ H_2O$, 2 g of $Co(NO_3)_2{\cdot}6\ H_2O$, and 0.84 g of urea were dissolved in deionized water, respectively. The solutions were thoroughly mixed and transferred to a 100 mL Teflon-lined stainless-steel autoclave, containing pretreated CC or CTC ($7\times7\ cm^2$). The autoclave was sealed and maintained at 160℃ for 6 h in an electric oven. After cooling to room temperature, CC or CTC was taken out and washed with water and ethanol. The obtained CC and CTC were calcined in air at 350°C for 2 h and were named $NiCo_2O_4$/CC and $NiCo_2O_4$/CTC, respectively.

2.3. Synthesis of UCAM

UCAM was fabricated by nonsolvent-induced phase separation (NIPS) method [22]. A uniform casting solution containing 8 g of polyvinylidene fluoride (PVDF), 0.2 g of polyvinyl pyrrolidone (PVP) and 50 mL of N, N-dimethylformamide (DMF) solution was spread on $NiCo_2O_4$/CC or $NiCo_2O_4$/CC that were fixed on a perforated stainless-steel plate using a casting knife with a gap of 500 μm. The casting knife was subsequently adjusted to a 250 μm gap, after which the casting solution was spread on it again. After that, the stainless-steel plate was immediately immersed in deionized (DI) water, forming an ultrafiltration-catalysis/adsorption microreactor (UCAM-CC/CTC). Finally, the prepared microreactor was immersed in DI water for 48 h to remove residual solvents and stored at 4–6℃ before use.

2.4. Characterizations and analysis

The morphology and elemental composition of the prepared materials were determined via transmission electron microscopy (TEM, JEM-2100 F, Japan) and scanning electron microscopy (SEM, JEM-7600 F, Japan) equipped with energy dispersive spectroscopy (EDS) mapping. The concentration of NDMA, *N*-nitrosodiethylamine (NPYR), *N*-nitrosopyrrolidine (NPYR), and *N*-nitrosodipropylamine (NDPA) in the simulated solution was measured by high-performance liquid chromatography (HPLC, Agilent 1260, USA) with a detection wavelength of 230 nm. The mobile phase used for NDMA, NDEA, and NPYR (NDPA) was an isocratic 80/20 (50/50) water/methanol mixture with a flow rate of 1 mL/min. Other characterization and analytical methods are described in the SI (Text S2, Table S2, 3, and Fig. S1).

2.5. Experiment

Batch experiments were conducted by the traditional bottle-point method in 100 mL of synthetic solution and then shaken in a thermostatic shaker (160 r/min) (pH=7.5±0.2; temperature: 25℃). The amount of materials used in all adsorption (catalysis) experiments was

set to 0.5 (0.1) g/L. Carbon-cloth-based microreactors ($NiCo_2O_4$/CC, $NiCo_2O_4$/CTC, UCAM-CC, and UCAM-CTC) use a filtration apparatus (Fig. 1a) in bottom-up mode to evaluate the adsorption or catalysis performance for *N*-nitrosamines and *N*-nitrosamine precursors. The concentration of pollutants in simulated water was 0.1 mmol/L. The detailed procedure of other experiments is presented in Text S2 in the SI.

2.6. Theoretical calculations

The combination of quantum chemical calculations and molecular dynamics simulation was adopted to reveal catalysis and adsorption mechanism. Details of the theoretical calculations are described in Text S3 in the SI.

3. Results and discussion

3.1. Characterizations

As shown in Fig. 1a, UCAM was prepared using carbon cloth as a substrate through hydrothermal, calcination and membrane encapsulation processes. A photo of the UCAM and the microstructure of the top surface were observed (Fig. S2), with surface pore sizes ranging from 20 to 30 nm. Moreover, the texture of carbon cloth can be clearly observed from the bottom of the UCAM, suggesting that a dense selection layer was not formed on the bottom. Meanwhile, the SEM image showed that the nanoparticles were covered by the membrane on the carbon cloth. This phenomenon proved that UCAM successfully encapsulated the modified carbon cloth and confined the material within the membrane to avoid the impact of the functional materials loss on its own properties and the water environment.

The SEM images of $NiCo_2O_4$/CC and $NiCo_2O_4$/CTC (Fig. 1b1 and S3) indicated that the entire fiber surfaces of CC and CTC (Fig. S4) were completely covered by crosslinked $NiCo_2O_4$-nanowires. Elemental mapping analysis exhibited the uniform distribution of $NiCo_2O_4$-nanowires on the interleaved carbon cloth matrix, which formed a functional network (Fig. 1b2 and S5). These rich array structures of nanowires provide abundant contact areas and multiple transport channels for pollutants during the reaction process. TEM provided additional information on the microstructure of $NiCo_2O_4$-nanowires (Fig. 1c). A single $NiCo_2O_4$-nanowire had an average diameter of more than 40 nm and high-resolution TEM image of the nanowires showed that the structure exhibited a lattice spacing of 2.45 Å, corresponding to the (311) facets of the $NiCo_2O_4$ spinel structure. Co, Ni, and O are uniformly dispersed on the nanowires (Fig. S6).

After constructing the reactor based on carbon cloth, its internal structure was examined through SEM of the UCAM cross section (Fig. 1d1). The thickness of the selective layer in the top part of the UCAM is approximately 30 nm, while the region below is the encapsulated functional layer of $NiCo_2O_4$/CC and $NiCo_2O_4$/CTC. The elemental mappings (Fig. 1d2) further validate the sequential spatial distribution

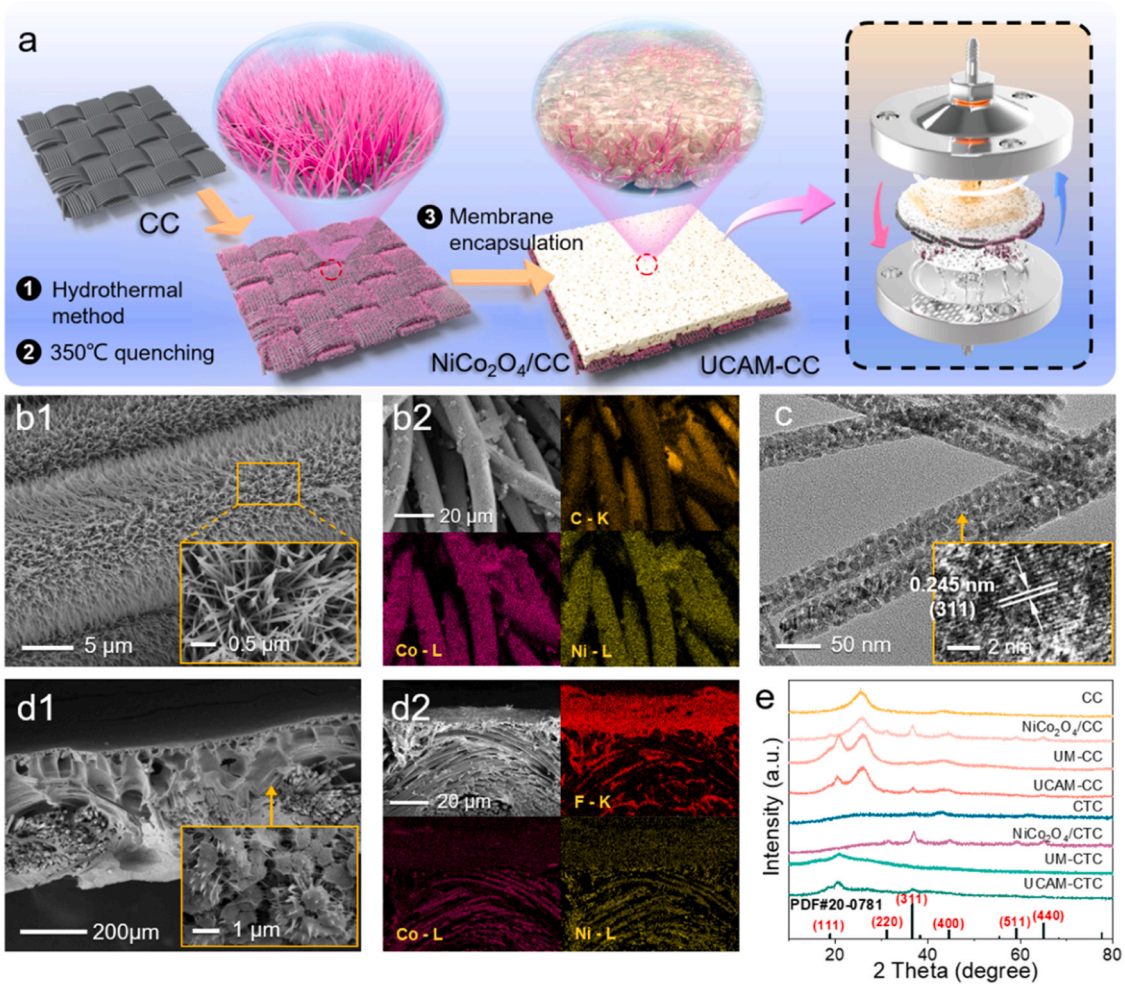

Fig. 1. (a) Schematic illustration of the synthesis pathway of UCAM; (b1) SEM image of $NiCo_2O_4$-nanoarrays on carbon fibers of $NiCo_2O_4$/CC and its enlarged image; (b2) elemental mappings of $NiCo_2O_4$/CC; (c) TEM image of $NiCo_2O_4$-nanoarrays and high-resolution maps; (d1) cross-section of UCAM-CC and its enlarged image; (d2) elemental mappings corresponding to the cross-section of UCAM-CC; (e) X-ray diffractometry (XRD) patterns of materials.

within the UCAM. The $NiCo_2O_4$-nanowires grown on carbon cloth are mainly distributed below the UCAM, corresponding to the Co and Ni signals. Moreover, the enlarged image (Fig. 1d1 and S7) demonstrates that the $NiCo_2O_4$-nanoarrays on the carbon cloth are encapsulated within the membrane, which increases the mass transfer of pollutants and results in the formation of a confined microreactor, leading to high catalysis and adsorption performance inside it.

The XRD results showed that the analogous characteristic peaks of $NiCo_2O_4$/CC and $NiCo_2O_4$/CTC matched a $NiCo_2O_4$ crystal (JCPDS Card No: 20–0781), indicating that the spinel type of $NiCo_2O_4$ grew well on the CTC and CC (Fig. 1e). In addition, $NiCo_2O_4$-related peaks still existed in the UCAM-CC and UCAM-CTC spectra, suggesting that $NiCo_2O_4$ maintained crystallinity during the process of membrane encapsulation [27]. Moreover, attenuated total reflectance fourier transform infrared spectroscopy revealed the presence of metal oxygen bonds in UCAM (Fig. S8) [28]. The similar pore size distributions of UCAM-CC and UCAM-CTC (Fig. S9) further confirmed the negligible influence of carbon cloth substrate on the upper surface structure.

3.2. Catalysis and Adsorption Performance

Firstly, the removal of *N*-nitrosamines and *N*-nitrosamine precursors by different metal oxides and double metal spinel oxides was compared and the detailed content was illustrated in Text S5 and Fig. S10-15 in the SI. Among them, $NiCo_2O_4$ exhibited faster degradation kinetics and better adsorption performance for degrading four selected *N*-nitrosamines and adsorbing corresponding degradation products that were DMA, diethylamine (DEA), dipropylamine (DPA), and pyrrolidine (PYR). Therefore, using carbon cloth as a substrate, $NiCo_2O_4$ synthesized on its surface forms a catalysis-adsorption layer, and $NiCo_2O_4$/CC was optimized by adjusting the synthesis parameters to achieve a high $NiCo_2O_4$-nanoarrays loading (Fig. S16 and Table S4). Then, a microreactor is constructed on it through membrane encapsulation. With a high water-flux of 157 L m^{-2} h^{-1}, this sequential structure of UCAM could reject most of humic acid (HA) and bovine serum albumin (BSA) (over 93%) at the initial selective separation layer (Fig. S17). The performance of $NiCo_2O_4$/CC and UCAM-CC was evaluated under a series of HA concentrations and the first-order kinetic model (Text S6) was used to compare the rate of NDMA degradation and DMA adsorption. When HA concentration increased to 15 mg/L, the catalysis and adsorption performance of UCAM were only slightly affected (Figs. 2a and 2b inset), and remained stable for a considerable time. In contrast, the removal rates of NDMA and DMA by $NiCo_2O_4$/CC were significantly affected. The first-order kinetic constant of degradation and adsorption decreased from 4.54 and 0.27 min^{-1} to 0.93 and 0.11 min^{-1}, respectively. Meanwhile, the *N*-nitrosamines removal efficiency gradually decreased with increasing treatment volume to 400 L m^{-2} (Fig. S18). The results illustrated that UCAM exhibits excellent antidisturbance performance in water remediation for multipollutant systems.

More importantly, UCAM-CC had a much greater NDMA removal efficiency than $NiCo_2O_4$/CC under the same conditions. The kinetic constants of NDMA degradation and DMA adsorption by UCAM-CC were 21.84 min^{-1} and 2.12 min^{-1}, respectively, which are approximately 5 and 8 times as much as those of $NiCo_2O_4$/CC. Under the interference of

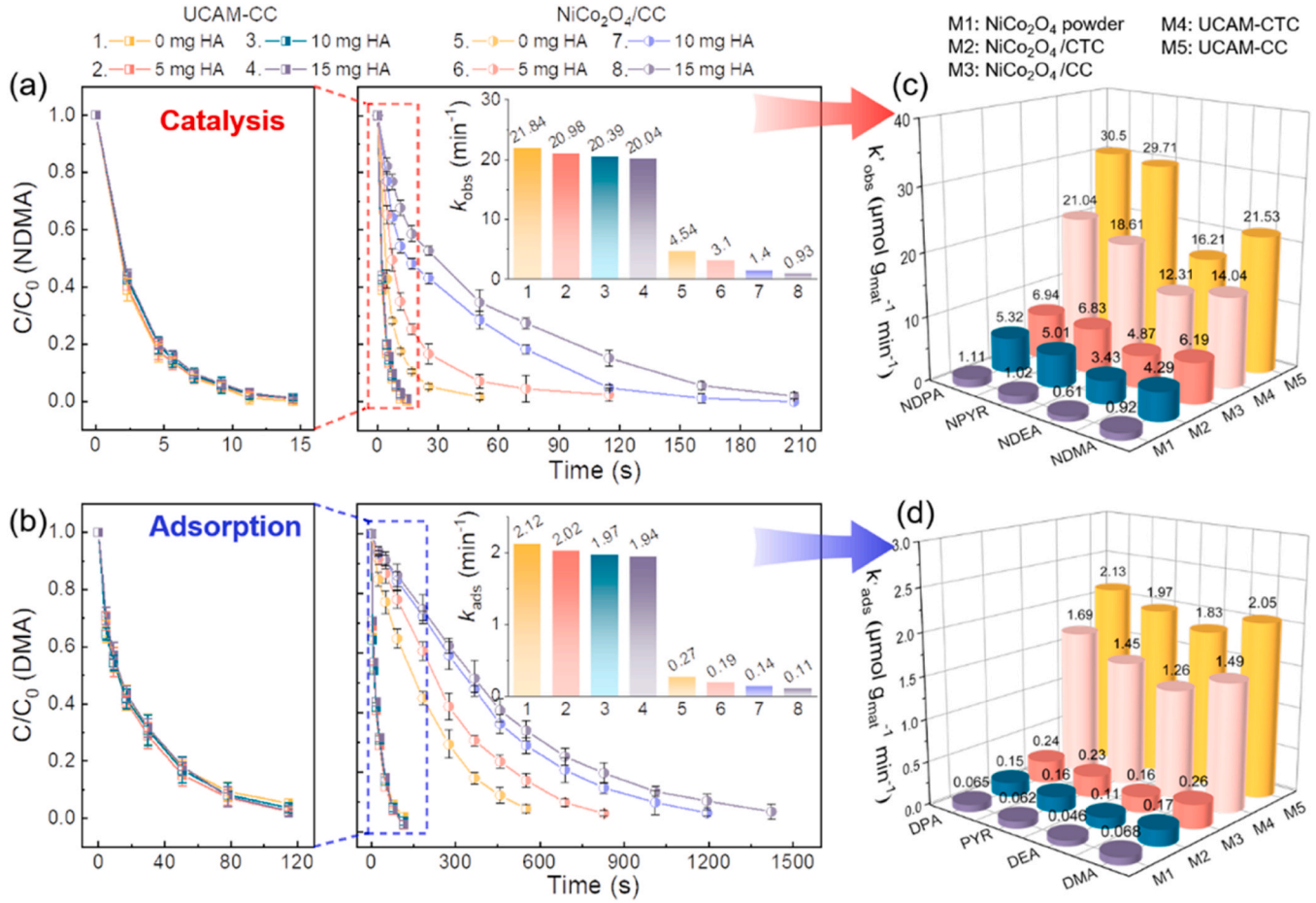

Fig. 2. (a) Effect of HA coexistence on NDMA degradation by $NiCo_2O_4$/CC and UCAM-CC with PMS activation; (b) effect of HA coexistence on DMA adsorption by $NiCo_2O_4$/CC and UCAM-CC; modified kinetic model (k') of (c) four *N*-nitrosamines degradation and (d) corresponding aliphatic secondary amine adsorption by M1, M2, M3, M4, and M5, corresponding to $NiCo_2O_4$ powder in the fixed-bed experiment and $NiCo_2O_4$/CTC, $NiCo_2O_4$/CC, UCAM-CTC, and UCAM-CC in the flow-through process. (Conditions: $[PMS]_0$=0.1 g L^{-1}, $[pollution]_0$=0.1 mmol L^{-1}, initial pH=7, temperature=25℃.).

HA, the kinetic constant of UCAM-CC is even over 21.5 times higher than that of $NiCo_2O_4$/CC. Additionally, the rate of degradation and adsorption of various materials (powder $NiCo_2O_4$, $NiCo_2O_4$/CC, $NiCo_2O_4$/CTC, UCAM-CC, and UCAM-CTC) was further evaluated by modified kinetic model (k') in Text S6 [27]. Both UCAM-CC and UCAM-CTC have excellent removal effects on *N*-nitrosamines and *N*-nitrosamine precursors (Fig. S19-20), and the k' values of the four *N*-nitrosamines and *N*-nitrosamine precursors treated with UCAM-CC are 22.2–28.1 and 29.2–38.8 times higher than powder $NiCo_2O_4$ in the traditional fixed bed treatment (Figs. 2c and 2d), showing the rapid degradation and adsorption capacity of UCAM in the flow filtration process.

However, the above studies separately discussed the removal of *N*-nitrosamines and *N*-nitrosamine precursors in byproduct. The behavior of UCAM in activating PMS to degrade *N*-nitrosamines while synchronously adsorbing secondary amines in the degradation products remains ambiguous.

As shown in Fig. 3a, three UCAMs were used to treat NDMA consecutively to further study the simultaneous degradation and adsorption processes. For comparison, NDMA degradation by $NiCo_2O_4$ was observed in static experiments (Fig. 3b). During the first 2 minutes, NDMA is rapidly degraded, and the byproducts are DMA, NO_2^-, NO_3^-, and a small amount of methylamine (MA). The concentration of DMA and dissolved organic nitrogen (DOC) gradually decreased over time, while that of NO_2^-, NO_3^- still increased, indicating that DMA was removed during the NDMA degradation. In contrast, degradation of NDMA by Co_3O_4 showed no significant decrease of DMA during the first 25 minutes (Fig. S21). Although the oxidation of *N*-nitrosamines releases some toxic nitrites, the influence of NO_2^- is negligible due to the presence of trace amounts of N-nitrosamines in real water (Fig. S22). To clarify the degradation pathway from NDMA to DMA in this system, liquid chromatograph mass spectrometer (LC-MS) analysis was employed (Fig. S23). Based on the detected intermediates, it was proposed that the degradation of NDMA to DMA can be classified into the cleavage of N-N bonds after hydroxylation and the direct cleavage of N-N bonds. Moreover, the C-N bond breaking during this process could lead to the generation of partial MA.

Fig. 3c shows that UCAM-1 achieves 98% degradation of NDMA after treatment, with subsequent UCAM-2 and UCAM-3 removing almost all remaining NDMA. However, DMA and MA in the UCAM-1 effluent accounted for 60.6% (54.8%+5.8%) of the initial NDMA content, and LC-MS analysis showed few other intermediates (Fig. S24). Therefore, the removal rate of DMA and MA was approximately 37% (98%-60.6%), which was lower than that of DMA by direct adsorption (~54%). This was attributed to the fact that NDMA degradation occurred prior to the adsorption of DMA. Most of NDMA was degraded, resulting in further removal of 49% DMA and MA from UCAM-2. After all treatments, the remaining DMA amount was less than 4%. These results show that UCAM-PMS system can synchronously remove NDMA and its byproducts as precursors, and present much greater removal effect even at lower concentration. Moreover, even with a treatment volume of 5000 L m^{-2}, UCAM-1 still achieved 93% NDMA removal, while UCAM-3 exceeded 99% removal efficiency (Fig. 3d). In contrast, the DMA contents in the effluent of UCAM-1, UCAM-2, and UCAM-3 increased to 13%, 37%, and 78%, respectively (Fig. 3d). As the effective adsorption sites tend to saturate, the adsorption efficiency of DMA significantly decreases. In addition, the activation of PMS may also affect DMA removal by UCAM, which will be discussed below.

An important aspect that affects the practical application of an

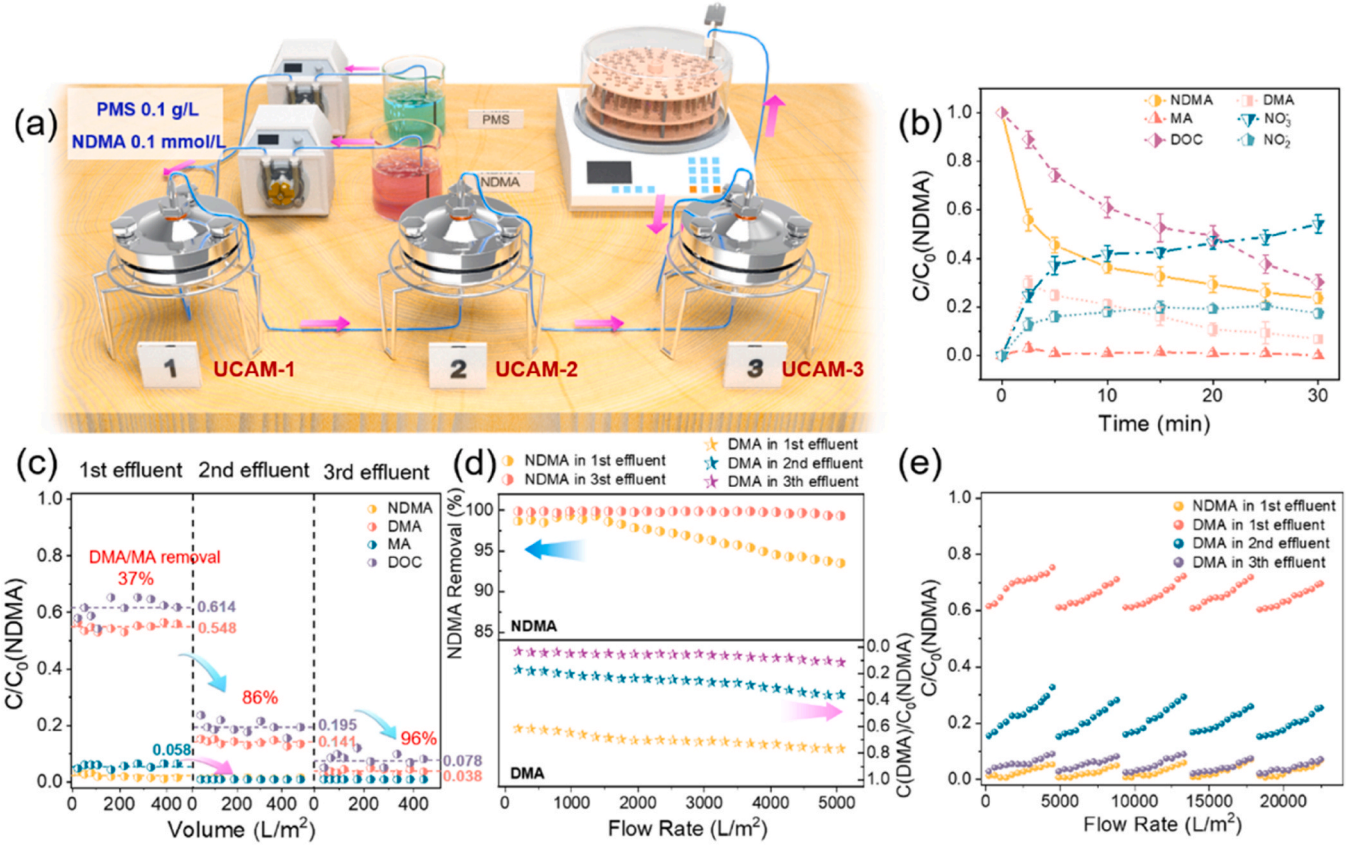

Fig. 3. (a) Schematic diagram of UCAM flow process treatment (PMS solution concentration: 2.0 g/L, corresponding peristaltic pump flow rate: 0.2 mL/min; NDMA solution concentration: 4.0 g/L, corresponding peristaltic pump flow rate: 4.0 mL/min); (b) changes in NDMA and its byproducts during PMS activation in batch experiment; (c) comparison of NDMA and its byproducts in the effluent of three sections; (d) the content of NDMA and DMA during flow process treatment; (e) performance of UCAM dynamic cycle experiment.

adsorbent or catalyst is the regeneration possibility. Herein, UCAM regeneration was conducted to maintain sustainable adsorption. UCAM maintains good removal performance for NDMA and DMA in 4 cycles of experiments (Fig. 3e). Interestingly, the adsorption performance of No.1, No.2 and No.3 UCAM showed an increasing trend in the last four cycles. During long-term operation, UCAM can maintain more than 98% NDMA and 90% DMA removal, demonstrating good stability. Moreover, another concern of using UCAM for actual water treatment is Ni and Co leaching. Therefore, the leached Ni and Co ion from effluent during continuous treatment was tested that the concentration of them was less than 0.01 and 0.08 mg L^{-1}, respectively (Fig. S25). This level is much lower than the environmental quality standards for surface water (0.02 mg for Ni^{2+} and 1 mg L^{-1} for Co^{2+}, GB 3838–2002, China). The low Co and Ni leaching is due to the encapsulation of the sequential microreactor, which avoids material loss in flowing water, thus ensuring the safety of the treatment process. The results indicates that UCAM is a promising material in wastewater treatment.

The relationship between adsorption and catalysis was further investigated in the treatment of NDMA. Fig. 4a illustrates that the coexistence of NDMA did not interfere with DMA adsorption, while PMS (0.1 g/L) slightly improves the DMA removal. When the PMS dose increased to 0.5 g/L, the improvement was still limited. However, PMS addition significantly boosts the effective treatment volume of UCAM for DMA (Fig. 4b). Meanwhile, the degradation of DMA by $NiCo_2O_4$ was investigated, and the DMA removal gradually increased with time (Fig. 4c). These results extrapolated that DMA adsorption by UCAM still dominated the DMA removal and the adsorbed DMA was further degraded with PMS activation, resulting in an increase in treatment volume of UCAM. Surprisingly, the DMA addition improved the degradation of NDMA (Fig. 4d). To investigate this phenomenon, the UCAM with pre-adsorption DMA was used to compare the catalytic performance. After processing DMA solution (1 L), UCAM exhibited much better NDMA removal performance than the original UCAM (Fig. 4d). With the accumulation of DMA by adsorption (after 5 L of processing), the catalytic performance also decreased, attributed to the saturation of UCAM with the DMA adsorption. Results indicated that the adsorbed DMA synergistically promoted the degradation of NDMA by UCAM.

The adsorption behavior of UCAM during catalysis-adsorption synergistic process was further examined using QCM-D (Fig. 4e), and the entire process can be divided into five stages. Initially, NDMA rapidly adsorbed onto $NiCo_2O_4$, with its concentration gradually decreasing after 4 minutes. Then, deionized water passed through the device upon frequency stabilization. In the second stage, a significant frequency shift occurred, indicating that the unstable interaction between NDMA and $NiCo_2O_4$ resulted in its easy desorption in water. In the third stage, the feed solution mixture of PMS and NDMA induced a rapid frequency shift change (Δf3), which decreased from -4.7 ± 0.9 Hz at 45 min to -58.6 ± 1.8 Hz at 93 min, primarily attributed to the adsorption of matter on the materials.

We further compared the adsorption of PMS and DMA on materials (Fig. 4f). PMS exhibited less significant adsorption (8.7 Hz frequency shift) due to its rapid activation after adsorption. The adsorption of DMA showed a rapid phase followed by slower adsorption and finally reached stability, which is a process of rapid surface adsorption, internal mass transfer, and adsorption saturation. The NDMA degradation process activated by PMS involved the adsorption of NDMA, PMS, and degradation byproducts (mainly DMA), for which the adsorption rate was significantly slower than that of direct DMA alone. In addition, the amount of adsorbed substances during this process exceeded the amount directly adsorbed. Considering that the adsorbed NDMA and PMS were eventually degraded and activated, most of the adsorbed substances were DMA and other byproducts. This result suggested that the material activated PMS for NDMA degradation and improved DMA adsorption, shedding light on its potential in water treatment.

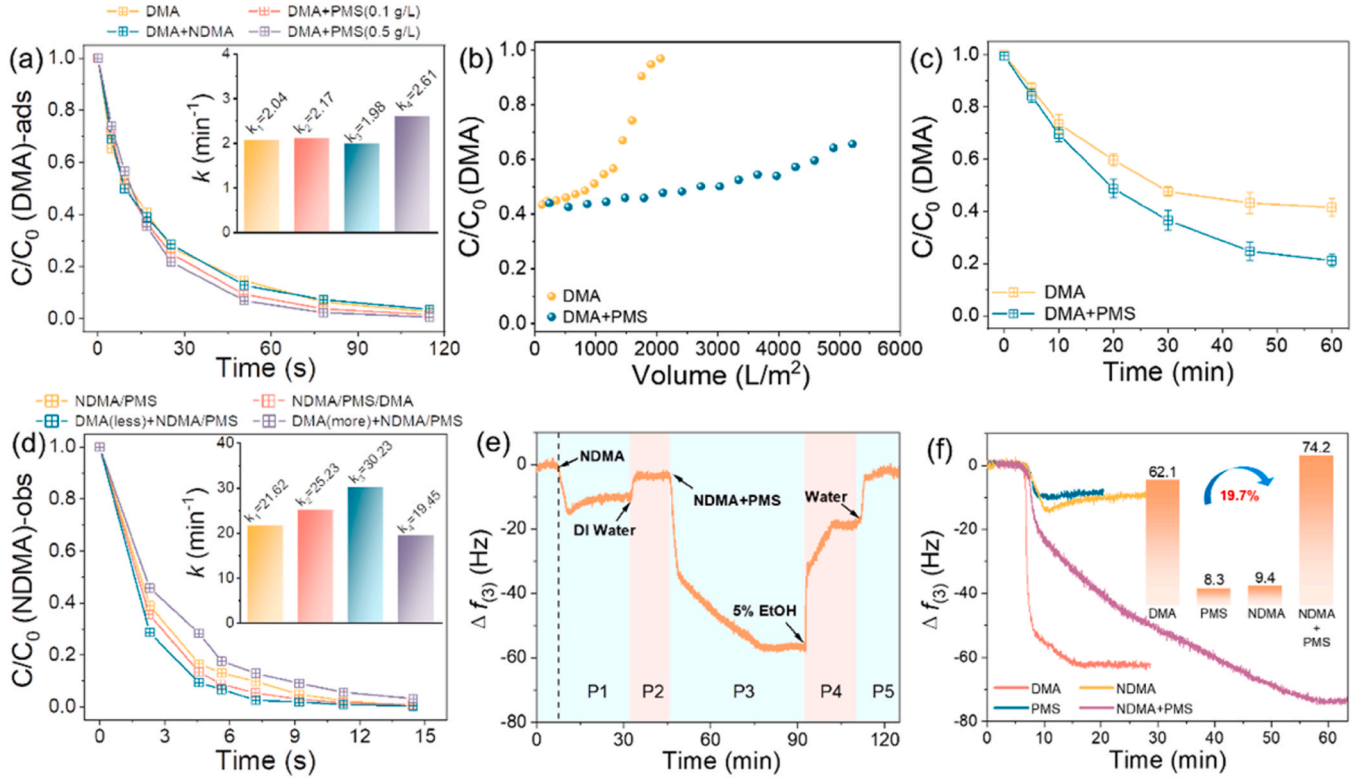

Fig. 4. (a) Effect of PMS and NDMA on DMA adsorption; effect of PMS on the removal of DMA by (b) UCAM and (c) $NiCo_2O_4$ powder; (d) effect of DMA adsorption on the NDMA oxidation; (e) representative third frequency shift for substances on $NiCo_2O_4$-coated quartz crystal microbalance (QCM) sensor surfaces at different stages; (f) comparison of the adsorption effect of $NiCo_2O_4$ on different substances.

3.3. Decontamination mechanism

The microreactor, constructed through membrane encapsulation, significantly improved the pollutant removal efficiency. Therefore, identifying the role of each component during the removal of *N*-nitrosamines via adsorption-catalysis is crucial for elucidating the underlying mechanism involved. Herein, we evaluated the removal on *N*-nitrosamines removal by UCAM-CC and UCAM-CTC under different condition. UCAM-CC and UCAM-CTC showed negligible *N*-nitrosamine removal without PMS addition (Fig. S26), indicating the weak interaction between *N*-nitrosamine and the material. Therefore, the *N*-nitrosamine adsorption on UCAM was negligible. In contrast, four *N*-nitrosamines were rapidly removed in the UCAM-PMS system. Meanwhile, the membrane encapsulated pure carbon cloth (UM) exhibited almost no removal of pollutants in the presence or absence of PMS addition (Fig. S26, S27), revealing that the carbon substrate and membrane substrate themselves do not have the pollutants adsorption or PMS activation capacity. Therefore, the effective removal of *N*-nitrosamines and secondary amines relies on the excellent PMS activation ability and special adsorption sites of $NiCo_2O_4$-nanoarrays on carbon cloth. Moreover, considering that HA were rejected on the surface of the selective layer, leading to the accumulation to form a filter cake layer and cause the possibility of adsorption to *N*-nitrosamines and corresponding precursors. Experiments revealed that UCAM, fouled by HA, did not affect the removal of *N*-nitrosamines or *N*-nitrosamine precursors other than NDPA or DPA, revealing that HA preseparation did not influence pollutant mass transfer during filtration (Fig. S28). The variation of the DPA and NDPA removal may be attributed to the interaction between their hydrophobic properties and the hydrophobic segments of humic acid.

The reported mechanisms of PMS activation can be categorized into radical (•OH and $SO_4^{\bullet-}$) and nonradical ($^1O_2$) processes [27]. To illuminate the mechanisms of *N*-nitrosamine degradation, scavenging experiments with the $NiCo_2O_4$-PMS and UCAM-PMS system were performed using methanol (MeOH) to capture •OH and $SO_4^{\bullet-}$, and tert-butanol (TBA) to efficiently capture •OH. The addition of TBA resulted in decreasing removal rate of NDMA from 75% to 66% (Fig. 5a), while only 10% of NDMA was degraded with the MeOH addition, suggesting that $SO_4^{\bullet-}$ plays a dominant role in the degradation. The use of 2,2,6,6-tetramethylpiperidine (TEMP) as a sacrificial agent for $^1O_2$ had an inhibitory effect, indicating the presence of $^1O_2$ in the system. A similar phenomenon was observed in the scavenging experiments for UCAM (Fig. S29). Furthermore, Electron paramagnetic resonance (EPR) spectroscopy that was used to directly detect the products of spin-trapping agents for reactive oxygen species also verified above opinion. 5,5-dimethyl-1-pyrroline-1-oxide (DMPO) and TEMP were used to detect the production of radicals and $^1O_2$, respectively. As shown in Fig. 5b, typical signals of DMPO-•OH were observed, and DMPO-$SO_4^{\bullet-}$ signals appeared around the •OH peaks, revealing the presence of •OH and $SO_4^{\bullet-}$. Meanwhile, the signal with TEMPO adducts indicated the generation of $^1O_2$. Overall, $SO_4^{\bullet-}$ played a dominant role in the degradation process with the existence of both radical and nonradical processes.

Electrochemical analysis demonstrated the electrochemical properties of the catalysts and the electron-transfer process. Electrochemical impedance spectroscopy (Fig. S30) showed that the electrons were more easily transferred at the interface of CC and CTC loaded with CoNi spinel

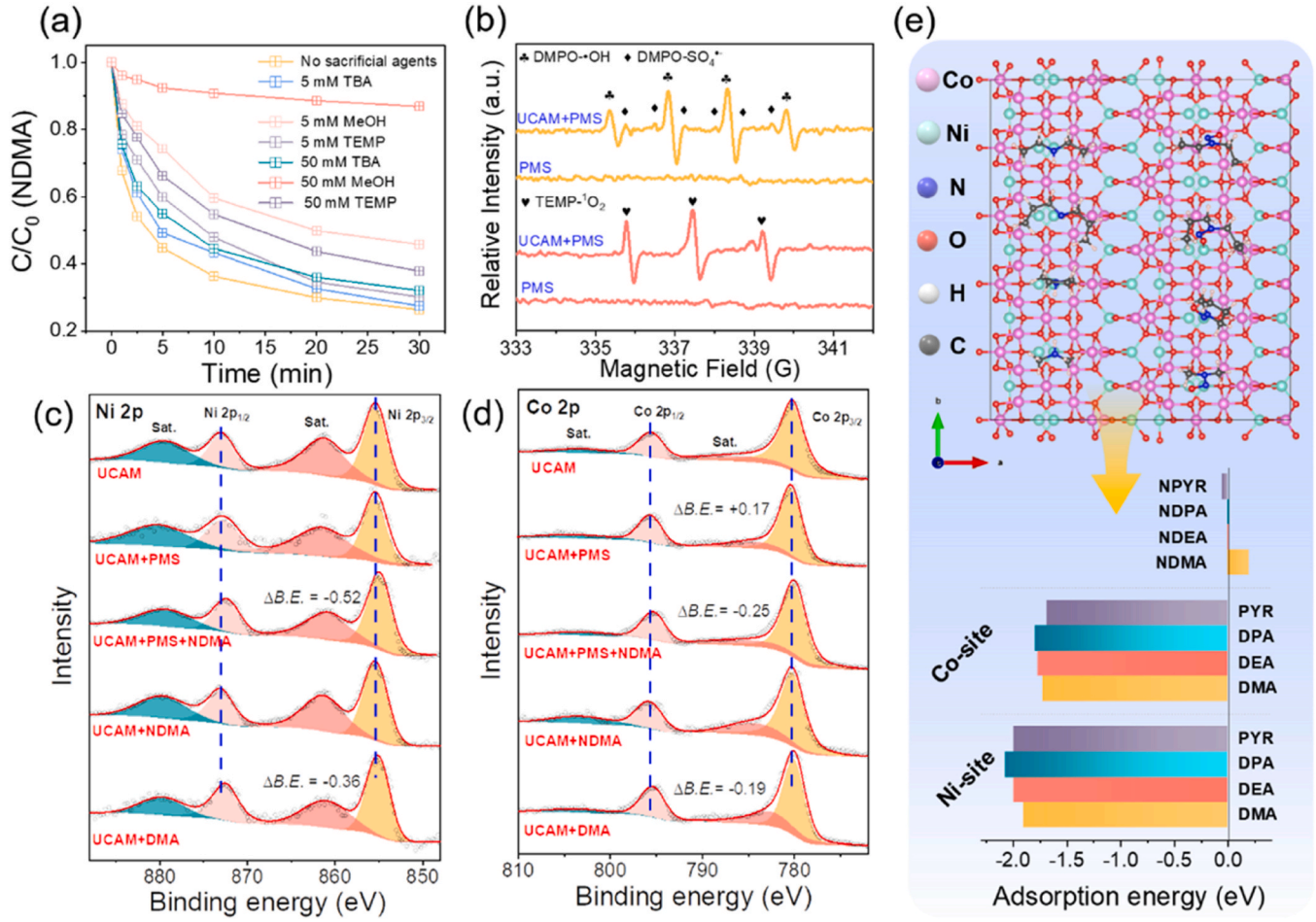

Fig. 5. (a) Effect of scavengers on NDMA degradation in $NiCo_2O_4$/PMS system; (b) EPR spectra of DMPO and TEMP in PMS activation systems; high-resolution XPS of the (c) Ni and (d) Co element in the UCAM before and after different reaction condition; (e) the adsorption energy between $NiCo_2O_4$ and pollutants.

oxide. Linear sweep voltammetry (LSV) curves showed that the current density obviously increased with the addition of PMS (Fig. S31). Then, another higher current was obtained when NDMA addition was triggered, indicating that the electric field was accelerated by the interaction between NDMA and $NiCo_2O_4$/CC-PMS system [29]. Chronoamperometry measurements demonstrated the electron-transfer during PMS activation (Fig. S32). The negative current peak upon PMS injection indicated an electron density change between the catalysts and PMS. Then, subsequent addition of four *N*-nitrosamines resulted in a decrease in the current density, revealing that the addition of pollutants suddenly accelerated the electron transfer from the electrochemical station to the $NiCo_2O_4$/CC working electrode. These results underscored that the material can activate PMS and degrade *N*-nitrosamines [11].

To delved into the role of Ni-Co in the catalytic-adsorption synergy, X-ray photoelectron spectroscopy (XPS) was conducted on UCAM before and after the reaction. Fig. S33 illustrates an increased proportion of Co^{3+}/Co^{2+} peak position after the reaction, which indicated that the Co site is involved in the activation of PMS and electron transfer occurs

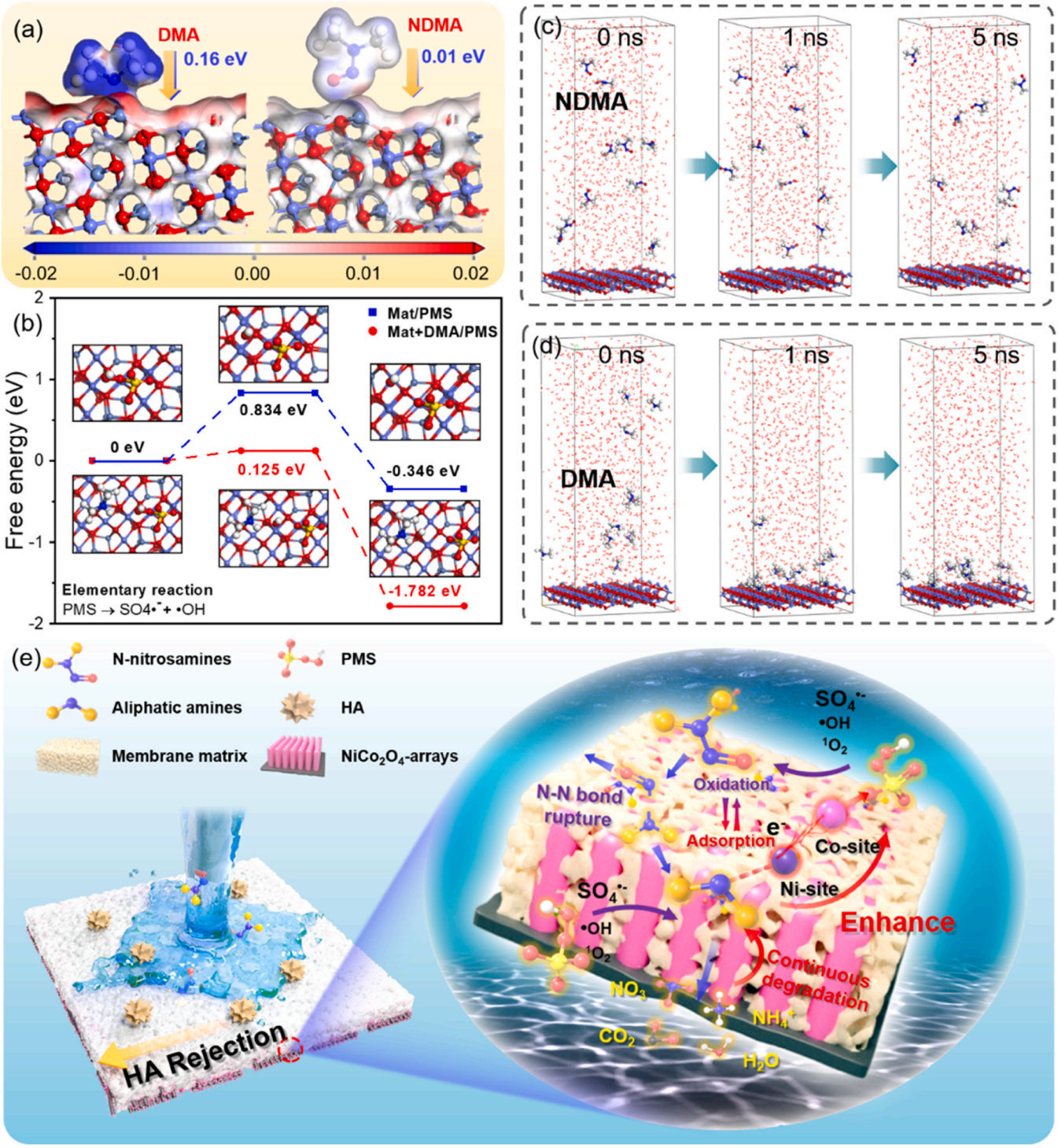

Fig. 6. (a) Charge difference of the DMA and NDMA adsorbed on $NiCo_2O_4$; (b) transition state theory of PMS activation reaction. (c, d) MD simulation analysis of adsorbate and adsorbent; (e) synergistic mechanism of removal of multiple pollutants.

[30]. Conversely, the Ni XPS showed a slight increase in the proportion of Ni^{2+} after the reaction, which was probably attributed to that the PMS system activated the conversion from Ni^{3+} to Ni^{2+} sites [15,30]. After the reactions, the content of the oxygen of the hydroxyl group adsorbed at the surface of catalysts increased compared with the lattice oxygen of metal oxides (Fig. S34). This was probably contributed by the hydroxyl group from dissociative adsorption of water molecules on transition metal oxides. Notably, the peak position of the Ni and Co both showed a lower energy shift after its reaction with different *N*-nitrosamines. Therefore, the changes in Ni 2p and Co 2p of $NiCo_2O_4$/CC before and after different reaction conditions were determined to study the inner mechanism (Figs. 5c and 5d). In the $NiCo_2O_4$/CC-NDMA system, almost no obvious changes occur in Ni and Co element, which also confirms the very weak interaction between the material and *N*-nitrosamines. However, with reaction with only PMS, there was no significant shift in the Ni element, and the peak position of Co element shifted to higher energy levels as a result of oxidation, indicating that Co sites are more likely to activation site of PMS. By contrast, after the adsorption of DMA and PMS+NDMA, both Ni and Co elements showed a shift towards lower energy, indicating that the Ni and Co sites received additional electrons [31]. The shift degree of Ni is significantly higher than that of Co, indicating that degraded secondary amine such as DMA are more easily adsorbed on Ni sites. Moreover, no significant change in O element occur in the system, indicating that the electrons did not come from the material [32]. Meanwhile, PMS hardly reduce Ni(II), indicating that the electron source was the *N*-nitrosamines or their byproduct [32]. Compared with the -NH- peak before reaction, the N analysis exhibited a new peak after adsorption, which was attributed to the complexation state between -NH- and the metal (Fig. S35). Therefore, the received electrons of Ni^{2+} originated from the lone pair of electrons (-NH-) in the degraded product. These interaction enable the material to effectively adsorb degradation products or other precursors. Moreover, the stronger displacement of Ni and Co after PMS activation also confirms the previous experiments that this material exhibited the better adsorption effect in degrading NDMA and adsorbing DMA than directly adsorbing DMA.

The above discussion was further validated using density function theory (DFT). Fig. 5e, S36 and S37 show that the adsorption energy of the model precursor on $NiCo_2O_4$ was much better than those of *N*-nitrosamines and carbon substrate showed poor affinity to both two kinds of pollutants. The binding energy of aliphatic amines at Ni sites exceeded that at Co sites, indicating that pollutant molecules are more likely to interact with Ni sites. Electron transfer calculations demonstrated that aliphatic amine loses electrons and transfers them to $NiCo_2O_4$, confirming complexation with the material. To verify this hypothesis, the charge difference of the system was calculated for pollutants adsorbed on Ni sites (Fig. 6a). With aliphatic amine adsorption, electrons were inject into Ni and transferred on the surface, resulting in an increased electron cloud density of Co [32]. However, only slight change occurred with *N*-nitrosamines existence. The electron donating effect provided by ligand-complexation may be the main reason for the excellent catalytic performance [33].

Transition state theory was used to determine the kinetics of PMS activation, revealing significant insights into the process. The energy barrier of PMS activation with the system of materials + DMA was lower than that of direct activating PMS activation with the materials, and had a lower reaction energy at the Co site. Moreover, the H atom in DMA could adsorb the OH radicals produced via PMS activation, thereby enhancing the catalytic activity. Ligand complexation from DMA activates the catalytic center and lowers the energy barrier for PMS activation, accelerating reactive oxygen species generation.

The above demonstrations verify the interaction between the material and the pollutants. Moreover, electrostatic potential analysis shows that N1 and N2 atoms of *N*-nitrosamines do not have strong electronegativity (Fig. S38), suggesting that *N*-nitrosamines have little effective binding sites. As the N-N bond breaks, the nitrogen on aliphatic amines shows strong nucleophilic reactivity and is prone to interact with Ni sites. Moreover, *N*-nitrosamine compounds with high E_{HOMO} (Fig. S39) and low energy gap (Table S5) are more vulnerable to attack [34]. Molecular dynamics simulation further proved that secondary amines from nitrosamine degradation can be better adsorbed than *N*-nitrosamines (Figs. 6c, 6d and S40), and the corresponding mean square displacement also showed better adsorption stability for secondary amines (Fig. S41). These calculation results were consistent with our hypothesis and revealed the synergistic effects of the selective adsorption and efficient catalytic degradation.

In summary, the synergistic mechanism of UCAM for complete removal of *N*-nitrosamines is shown in Fig. 6e. The reactor not only provides interference protection, but also significantly improves the removal of *N*-nitrosamines by encapsulating dispersed materials to construct a microreactor. The CoNi spinel oxide in the internal rapidly degraded *N*-nitrosamines into secondary amines. Moreover, the Ni sites on the material effectively adsorb secondary amines while synergistically enhancing PMS activation. The adsorbed DMA was mineralized during continuous activation, improving the adsorption performance of UCAM. This synergetic adsorption-catalysis approach ultimately promotes the complete removal of *N*-nitrosamines at the CoNi-oxide interface.

3.4. Potential application in wastewater

Widespread anions in wastewater have some interference on the treatment process. Herein, the effect of relevant anions on the removal of NDMA was investigated in the UCAM/PMS system (Fig. S42). Compared with that of the other anions, the degradation was slightly impacted with the addition of HCO_3^-, which may be attributed to the reaction of HCO_3^- with radicals. However, the effective immobilization structure of this microreactor can replenish the consumed radicals in a short period of time, thereby reducing the inhibitory effect of HCO_3^-. Therefore, UCAM has adaptability to saline wastewater.

To assess the stability of UCAM, real industrial wastewater was selected as the reaction solution, and changes in parameters such as NDMA were monitored during a continuous 30-day treatment process (Fig. 7a and S43). Ultrafiltration membrane treatment was used for comparison. During the UCAM-PMS treatment, the concentration of NDMA decreased from approximately 0.217 to 0.012±0.006 μg/L (removal rate reached 94.4%). Conversely, the NDMA content after ultrafiltration was still 0.199±0.031 μg/L. UCAM exhibited significant degradation of trace *N*-nitrosamines and excellent stability under long-term operation. Moreover, dissolved organic matter (DOM) is considered an important precursor of disinfection byproducts. DOC concentration decreased from 8.12 mg/L to 3.56 mg/L after ultrafiltration, indicating that membrane treatment eliminated approximately 60% of DOM while small organic molecule could still penetrate the membrane. These low-molecular-weight DOM (humic and protein substances) contributed more to the formation of *N*-nitrosamine disinfection byproducts [35]. After catalysis-adsorption treatment of UCAM, the DOC concentration decreased to 1.32 mg/L, indicating that more than 70% of this portion of organic matter was further adsorbed or mineralized. To further understand its composition, excitation-emission matrix (EEM) experiments and parallel factor analysis (PARAFAC) were conducted on the water samples based on relevant research (Fig. S44, S45) [36]. Compared to ultrafiltration, the fluorescence intensity of raw water significantly decreased after treatment with the UCAM/PMS system. EEM-PARAFAC divided dissolved fluorescent organic matter into three components: C1 (tyrosine protein-like), C2 (tryptophan protein-like), and C3 (humic-like) and performed normalization analysis [37]. During the membrane treatment process, the content of C3 decreased significantly by 72%, while the content of C1 and C2 components decreased by only 19% and 15%, respectively. In contrast, the removal rates of C1, C2, and C3 were 64%, 76%, and 84% in the UCAM/PMS system, indicating that the catalysis-adsorption process can

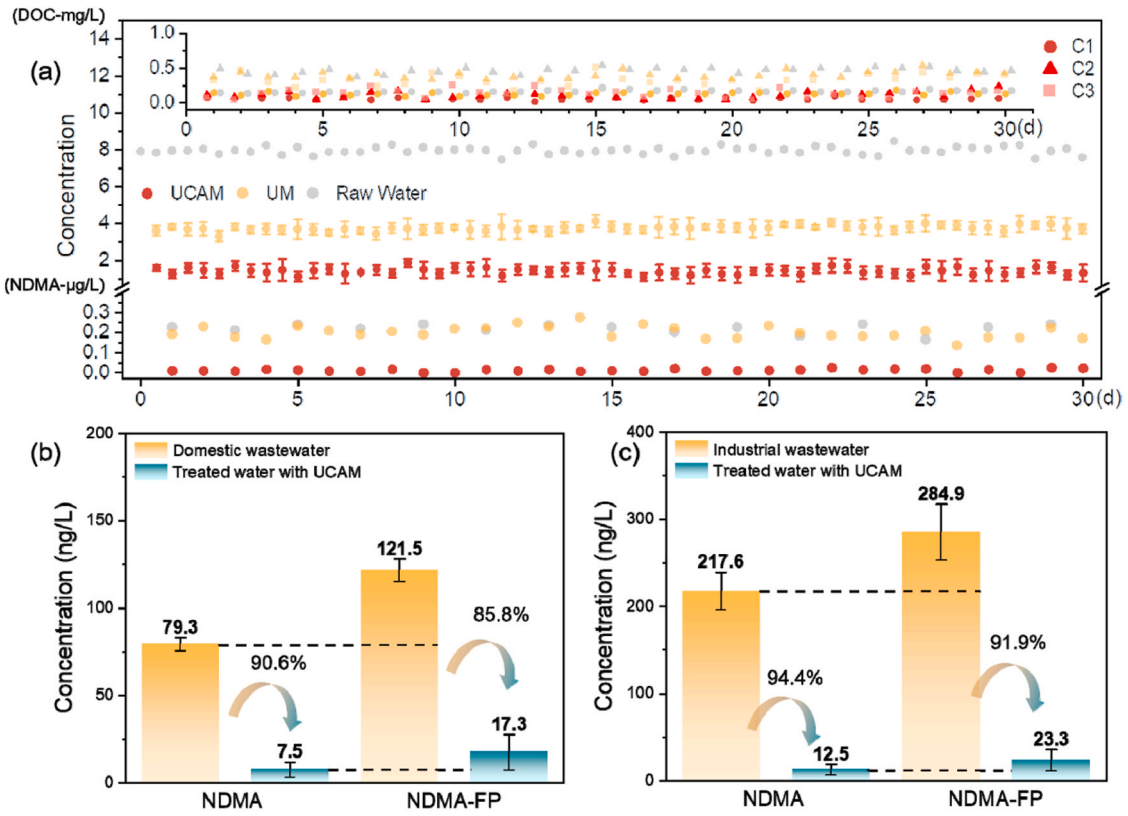

Fig. 7. (a) DOC and NDMA concentration in the effluent during the 30-day continuous treatment with UCAM/PMS and UM; the inner diagram showed the corresponding changes in fluorescence composition daily. Comparison of average NDMA concentration and NDMA-FP in (b) industrial wastewater and (c) domestic wastewater before and after UCAM/PMS treatment.

further efficiently remove low molecular-weight NOM, especially protein-like components. The NDMA-FP test showed a 91.1% reduction in NDMA-FP after treatment, suggesting over 90% removal of precursors (Fig. 7b). The experiment revealed that the majority of NDMA was degraded during the UCAM treatment process, and abundant *N*-nitrosamine precursors were removed, controlling the formation of *N*-nitrosamine disinfection byproducts and realizing complete *N*-nitrosamine removal. This technology has demonstrated excellent efficacy in treating *N*-nitrosamines and their precursors that rivals or even surpasses reported reverse osmosis membrane [38]. Similarly, we selected another domestic sewage source in Nanjing and found that the UCAM-PMS still had good control effects on its NDMA and NDMA-FP (Fig. 7c).

UCAM has good self-cleaning properties due to the radical catalytic process itself. After cleaning, the water flux of the BSA contaminated UCAM significantly recovered and remained nearly equal to the initial flux after multiple cycles (Fig. S46). In addition, UCAM still maintains good removal efficiency for *N*-nitrosamines after bending or long-term soaking in water, proving its excellent stability (Fig. S47). Meanwhile, carbonized cotton cloth prepared from discarded cotton cloth can achieve low-cost large-scale synthesis of UCAM for actual water treatment (Fig. S48). It can be said that the UCAM/PMS system combines ultrafiltration, catalysis, and adsorption to efficiently and completely remove *N*-nitrosamines. Moreover, the combination of membrane technology and functional materials provides a new strategy for rapid removal of multiple pollutants in complex environments.

4. Conclusion

In view of difficulty in adsorbing *N*-nitrosamines and mineralizing *N*-nitrosamines precursors, we designed an integrative microreactor supported by carbon fiber cloth that integrated ultrafiltration and oxidation-adsorption orderly into one unit for complete and efficient control of *N*-nitrosamines. This sequential structure eliminates the interference of macromolecular pollutants in wastewater and achieves the dispersion and immobilization of nanomaterials. The CoNi spinel-type oxide dispersed on the carbon cloth surface activated PMS to degrade *N*-nitrosamines and selectively adsorb aliphatic amines in degradation products and *N*-nitrosamine precursors in wastewater, preventing their transformation into *N*-nitrosamines during subsequent disinfection. Meanwhile, the adsorbed degradation products on Ni sites served as electron donors that reconstructed the charge on the CoNi sites, reducing the energy barrier for PMS activation. The synergistic effects of adsorption and catalysis further improve the efficiency of removing *N*-nitrosamines and their precursors. The microreactive interface formed by the constructed microreactor and $NiCo_2O_4$-nanoarrays can significantly enhance the adsorption and catalytic performance of the material itself. The degradation kinetics of four *N*-nitrosamines and the adsorption kinetics of the corresponding aliphatic amines in degradation products with the microreactor were 22.2–28.1 and 29.2–38.8 times greater than those with the traditional fixed bed treatment, respectively. After 30 days of continuous operation, the removal rates of NDMA and NDMA-FP in wastewater still exceeded 90%. Considering the controllable synthesis, the design of this microreactor is also suitable for other environmental remediation methods. This strategy has guiding significance for synergistic removal of *N*-nitrosamines and their precursors and control of *N*-nitrosamine formation.

CRediT authorship contribution statement

Zifan Liu: Writing – original draft, Visualization, Methodology, Investigation, Formal analysis, Data curation, Conceptualization. **Yu Meng:** Visualization, Formal analysis, Data curation. **Yue Wang:** Investigation, Data curation, Conceptualization. **Fuqiang Liu:** Writing – review & editing. **Weiben Yang:** Writing – review & editing,

Investigation, Funding acquisition, Data curation, Conceptualization. **Zhonglong Yin:** Writing – review & editing, Funding acquisition. **Yong Dai:** Writing – review & editing. **Zepeng Zhang:** Visualization, Methodology.

Declaration of Competing Interest

The authors declare that they have no known competing financial interests or personal relationships that could have appeared to influence the work reported in this paper.

Data Availability

No data was used for the research described in the article.

Acknowledgments

This research was financially funded by the Natural Science Foundation of China (Nos. 52070100 and 52200058).

Appendix A. Supporting information

Supplementary data associated with this article can be found in the online version at doi:10.1016/j.apcatb.2024.124219.

References

[1] A. Szczuka, N. Huang, J.A. MacDonald, A. Nayak, Z. Zhang, W.A. Mitch, N-Nitrosodimethylamine formation during UV/Hydrogen peroxide and UV/Chlorine advanced oxidation process treatment following reverse osmosis for potable reuse, Environ. Sci. Technol. 54 (2020) 15465–15475.

[2] W. Chen, Y. Chen, H. Huang, Y. Lu, M.S. Khorram, W. Zhao, D. Wang, S. Qi, B. Jin, G. Zhang, Occurrence of *N*-Nitrosamines in the pearl river delta of China: characterization and evaluation of different sources, Water Res 164 (2019) 114896.

[3] E.L. Marron, W.A. Mitch, U.V. Gunten, D.L. Sedlak, A tale of two treatments: the multiple barrier approach to removing chemical contaminants during potable water reuse, Acc. Chem. Res. 52 (2019) 615–622.

[4] J. Xie, Z. Lv, L. Ni, H. Zhang, X. Yan, Y. Zhou, Z. Zhu, J. Qi, X. Sun, J. Li, Synergies of the direct electrochemical reduction and Pd-Catalyzed hydrogenation in a sequential membrane for an efficient *N*-Nitrosodimethylamine removal, ACS EST Eng. 3 (2023) 1022–1029.

[5] J. McCutcheon, M. Mauter, Fixing the desalination membrane pipeline materials discovery alone has not translated into lower-cost water treatment, Science 380 (2023) 6642.

[6] C. Liu, M. Zhang, H. Gao, L. Kong, S. Fan, L. Wang, H. Shao, M. Long, X. Guo, Cyclic coupling of photocatalysis and adsorption for completely safe removal of *N*-nitrosamines in water, Water Res 209 (2021) 117904.

[7] S.W. Krasner, W.A. Mitch, D.L. McCurry, D. Hanigan, P. Westerhoff, Formation, precursors, control, and occurrence of nitrosamines in drinking water: a review, Water Res 47 (2013) 4433–4450.

[8] J. Lv, Y. Li, Y. Song, Reinvestigation on the ozonation of *N*-nitrosodimethylamine: Influencing factors and degradation mechanism, Water Res 47 (2013) 4993–5002.

[9] M. Davie, M. Reinhard, J. Shapley, Metal-Catalyzed reduction of *N*-Nitrosodimethylamine with hydrogen in water, Environ. Sci. Technol. 40 (2006) 7329–7335.

[10] Y. Wang, Y. Ge, R. Wang, Z. Liu, Z. Yin, Z. Yang, F. Liu, W. Yang, MOF-Derived Ni/ZIF-8/ZnO arrays on carbon fiber cloth for efficient adsorption-catalytic oxidation, Small 19 (2023) e2303928.

[11] M.M. Wang, L.J. Liu, J.T. Wen, Y. Ding, J.R. Xi, J.C. Li, F.Z. Lu, W.K. Wang, J. Xu, Multimetallic CuCoNi oxide canowires in situ grown on a nickel foam substrate catalyze persulfate activation via mediating electron transfer, Environ. Sci. Technol. 56 (2022) 12613–12624.

[12] Z. Liu, Z. Yin, Z. Zhang, C. Gao, Z. Yang, W. Yang, Removal of aliphatic amines by NiLa-Layered double hydroxide nanostructures, ACS Appl. Nano Mater. 5 (2022) 8120–8130.

[13] W. Beita-Sandi, M.S. Ersan, H. Uzun, T. Karanfil, Removal of *N*-nitrosodimethylamine precursors with powdered activated carbon adsorption, Water Res 88 (2016) 711–718.

[14] G. Anipsitakis, D. Dionysios, Radical generation by the interaction of transition metals with common oxidants, Environ. Sci. Technol. 38 (2004) 3705–3712.

[15] M. Wang, Y. Cui, H. Cao, P. Wei, C. Chen, X. Li, J. Xu, G. Sheng, Activating peroxydisulfate with $Co_3O_4/NiCo_2O_4$ double-shelled nanocages to selectively degrade bisphenol A – A nonradical oxidation process, Appl. Catal. B Environ. 282 (2021) 119585.

[16] B. Mahata, K. Chung, S. Chang, Removal of ammonium nitrogen (NH_4^+-N) by Cu-loaded amino-functionalized adsorbents, Chem. Eng. J. 411 (2021) 128589.

[17] B.C. Hodges, E.L. Cates, J.H. Kim, Challenges and prospects of advanced oxidation water treatment processes using catalytic nanomaterials, Nat. Nanotechnol. 13 (2018) 642–650.

[18] Y. Zhang, B. Pan, C. Shan, X. Gao, Enhanced phosphate removal by nanosized hydrated La(III) oxide confined in cross-linked polystyrene networks, Environ. Sci. Technol. 50 (2016) 1447–1454.

[19] P. Westerhoff, G. Aiken, G. Amy, J. Debroux, Relationships between the structure of natural organic matter and its reactivity towards molecular ozone and hydroxyl radicals, Water Res 33 (1999) 2265–2276.

[20] N. Li, X. Lu, M. He, X. Duan, B. Yan, G. Chen, S. Wang, Catalytic membrane-based oxidation-filtration systems for organic wastewater purification: A review, J. Hazard. Mater. 414 (2021) 125478.

[21] C. Chen, L. Lu, L. Fei, J. Xu, B. Wang, B. Li, L. Shen, H. Lin, Membrane-catalysis integrated system for contaminants degradation and membrane fouling mitigation: A review, Sci. Total. Environ. 904 (2023) 166220.

[22] S. Zhou, J. Zhu, Z. Wang, Z. Yang, W. Yang, Z. Yin, Defective MOFs-based electrocatalytic self-cleaning membrane for wastewater reclamation: Enhanced antibiotics removal, membrane fouling control and mechanisms, Water Res 220 (2022) 118635.

[23] M. Long, J. Donoso, M. Bhati, W.C. Elias, K.N. Heck, Y.H. Luo, Y.S. Lai, H. Gu, T. P. Senftle, C. Zhou, M.S. Wong, B.E. Rittmann, Adsorption and reductive defluorination of perfluorooctanoic acid over palladium nanoparticles, Environ. Sci. Technol. 55 (2021) 14836–14843.

[24] P. Gayen, C. Chen, J.T. Abiade, B.P. Chaplin, Electrochemical oxidation of atrazine and clothianidin on Bi-doped SnO_2-Ti_nO_{2n-1} electrocatalytic reactive electrochemical membranes, Environ. Sci. Technol. 52 (2018) 12675–12684.

[25] X. Lei, Y. Lei, J. Guan, P. Westerhoff, X. Yang, Kinetics and transformations of diverse dissolved organic matter fractions with sulfate radicals, Environ. Sci. Technol. 56 (2022) 4457–4466.

[26] J. Lee, U. von Gunten, J.H. Kim, Persulfate-based advanced oxidation: Critical assessment of opportunities and roadblocks, Environ. Sci. Technol. 54 (2020) 3064–3081.

[27] J. Xie, Z. Liao, M. Zhang, L. Ni, J. Qi, C. Wang, X. Sun, L. Wang, S. Wang, J. Li, Sequential ultrafiltration-catalysis membrane for excellent removal of multiple pollutants in water, Environ. Sci. Technol. 55 (2021) 2652–2661.

[28] C.T. Vu, T. Wu, Magnetic porous NiLa-Layered double oxides (LDOs) with improved phosphate adsorption and antibacterial activity for treatment of secondary effluent, Water Res 175 (2020) 115679.

[29] Y. Wang, Z. Zhang, Z. Yin, Z. Liu, Y. Liu, Z. Yang, W. Yang, Adsorption and catalysis of peroxymonosulfate on carbocatalysts for phenol degradation: The role of pyrrolic-nitrogen, Appl. Catal. B Environ. 319 (2022) 121891.

[30] M. Xu, H. Zhou, Z. Wu, N. Li, Z. Xiong, G. Yao, B. Lai, Efficient degradation of sulfamethoxazole by $NiCo_2O_4$ modified expanded graphite activated peroxymonosulfate: Characterization, mechanism and degradation intermediates, J. Hazard. Mater. 399 (2020) 123103.

[31] M. Shao, F. Ning, J. Zhao, M. Wei, D.G. Evans, X. Duan, Preparation of Fe_3O_4@SiO_2@layered double hydroxide core-shell microspheres for magnetic separation of proteins, J. Am. Chem. Soc. 134 (2012) 1071–1077.

[32] Z. Chen, F. An, Y. Zhang, Z. Liang, W. Liu, M. Xing, Single-atom Mo-Co catalyst with low biotoxicity for sustainable degradation of high-ionization-potential organic pollutants, Proc. Natl. Acad. Sci. U. S. A. 120 (2023) e2305933120..

[33] J. Zhang, C. Shan, W. Zhang, B. Pan, In situ ligand-modulated activation of inert Ce (III/IV) into ozonation catalyst for efficient water treatment, Proc. Natl. Acad. Sci. U. S. A. 120 (2023) e2305255120.

[34] Z.H. Xie, C.S. He, H.Y. Zhou, L.L. Li, Y. Liu, Y. Du, W. Liu, Y. Mu, B. Lai, Effects of molecular structure on organic contaminants' degradation efficiency and dominant ROS in the advanced oxidation process with multiple ROS, Environ. Sci. Technol. 56 (2022) 8784–8795.

[35] J. Peng, H. Huang, Y. Zhong, R. Yin, Q. Wu, C. Shang, X. Yang, Transformation of dissolved organic matter during biological wastewater treatment and relationships with the formation of nitrogenous disinfection byproducts, Water Res 222 (2022) 118870.

[36] T. Maqbool, J. Zhang, Y. Qin, Q.V. Ly, M.B. Asif, X. Zhang, Z. Zhang, Seasonal occurrence of *N*-nitrosamines and their association with dissolved organic matter in full-scale drinking water systems: Determination by LC-MS and EEM-PARAFAC, Water Res 183 (2020) 116096.

[37] H. Lin, L. Guo, Variations in Colloidal DOM Composition with Molecular Weight within Individual Water Samples as Characterized by Flow Field-Flow Fractionation and EEM-PARAFAC Analysis, Environ. Sci. Technol. 54 (2020) 1657–1667.

[38] T. Fujioka, K.P. Ishida, T. Shintani, H. Kodamatani, High rejection reverse osmosis membrane for removal of *N*-nitrosamines and their precursors, Water Res 131 (2018) 45–51.